Front. Optoelectron. 2016, 9(1): 71–80
DOI 10.1007/s12200-016-0566-7

RESEARCH ARTICLE

High-performance, stable and low-cost mesoscopic perovskite ($CH_3NH_3PbI_3$) solar cells based on poly(3-hexylthiophene)-modified carbon nanotube cathodes

Xiaoli ZHENG, Haining CHEN, Zhanhua WEI, Yinglong YANG, He LIN, Shihe YANG (✉)

Department of Chemistry, The Hong Kong University of Science and Technology, Clear Water Bay, Kowloon, Hong Kong, China

Abstract This work explores the use of poly(3-hexylthiophene) (P3HT) modified carbon nanotubes (CNTs@P3HT) for the cathodes of hole transporter free, mesoscopic perovskite ($CH_3NH_3PbI_3$) solar cells (PSCs), simultaneously achieving high-performance, high stability and low-cost PSCs. Here the thin P3HT modifier acts as an electron blocker to inhibit electron transfer into CNTs and a hydrophobic polymer binder to tightly cross-link the CNTs together to compact the carbon electrode film and greatly stabilize the solar cell. On the other hand, the presence of CNTs greatly improve the conductivity of P3HT. By optimizing the concentration of the P3HT modifier (2 mg/mL), we have improved the power conversion efficiencies (PCEs) of CNTs@P3HT based PSCs up to 13.43% with an average efficiency of 12.54%, which is much higher than the pure CNTs based PSCs (best PCE 10.59%) and the sandwich-type P3HT/CNTs based PSCs (best PCE 9.50%). In addition, the hysteresis of the CNTs@P3HT based PSCs is remarkably reduced due to the intimate interface between the perovskite and CNTs@P3HT electrodes. Degradation of the CNTs@P3HT based PSCs is also strongly retarded as compared to cells employing the pure CNTs electrode when exposed to the ambient condition of 20% – 40% humidity.

Keywords poly(3-hexylthiophene) (P3HT), carbon nanotube, $CH_3NH_3PbI_3$, mesoscopic perovskite solar cell (PSC), carbon cathode

1 Introduction

Mesoscopic perovskite solar cells (PSCs) have raised great interest for their simple fabrication process and relatively high power conversion efficiency (PCE) [1–9]. The most commonly reported structure of the mesoscopic PSCs is mainly composed of transparent conductive substrates (fluorine-doped tin oxide (FTO) or indium-doped tin oxide (ITO) glass), hole blocking layer (compact TiO_2 film), mesoscopic metal oxide scaffold layer (mostly used mesoporous TiO_2), light harvesting perovskite layer (such as $CH_3NH_3PbI_3$), hole-transporting material (HTM) layer and metal electrode, and has achieved the certified champion 20.1% PCE [10,11]. However, two current challenges may hinder the possible commercialization of the PSCs: 1) expensive organic HTM such as 2,2′,7,7′-Tetrakis[*N*,*N*-di(4-methoxyphenyl)amino]-9,9′-spirobifluorene (spiro-MeOTAD) with poor stability and 2) complicated vacuum evaporation process involves in the noble metal electrode deposition [12–15]. Consequently, replacing the high cost HTM and precious metal electrode with low cost and abundant materials has become an urgent issue.

Indeed, carbonaceous nanomaterials based PSCs (C-PSCs) have opened up a new direction for low-cost and high-efficiency PSCs, thanks to the high work function, high conductivity, high chemical stability, abundant supply and simple fabrication process of carbon materials [16–19]. These unique properties have allowed to use the carbonaceous materials to replace the precious metal cathode without even using the high-cost HTM [14]. Till present, tremendous efforts have been made to utilize various carbon nanomaterials including carbon nanoparticles, carbon nanotubes (CNTs), graphene and their mixtures as the counter electrodes of C-PSCs [20–26]. However, there are also several challenges with the C-PSCs: 1) poor film-formability of pure carbon materials, which may induce discontinuous conductive channels and thus lower the short-circuit photocurrent density (J_{sc}), 2) large sizes of carbon materials lead to poor interface with

Received December 1, 2015; accepted December 18, 2015

E-mail: chsyang@ust.hk

perovskite layer, increasing the recombination rate and thus lowing the open-circuit voltage (V_{oc}) and fill factor (*FF*), and 3) macro-/mesopores formed in a loosely packed carbon electrode may be susceptible to moisture penetration into the perovskite layer, decreasing the cell stability [27]. Recently, great efforts have been devoted to develop a variety of approaches for optimizing the efficiency and stability of the C-PSCs [28]. Han et al. have first developed a screen-printing technique to prepare fully printable HTM-free mesoscopic C-PSCs and adjusted compositions, sizes and thicknesses of mesoporous carbon electrodes to optimize the efficiency and stability of the C-PSCs, but high temperature calcination was needed for the carbon films [29–32]. We have developed an embedment method for the perovskite conversion resulting in high *FF* due to the excellent interface contact between perovskite and carbon electrode, but the cell efficiency remains to be improved owing to the loosely packed carbon materials [33]. Direct deposition of carbon materials onto preformed perovskite layers has also been explored at low temperature, but the *FF* is limited because of the non-ideal interface between the carbon electrode and perovskite [34–36]. To tackle the film-formation and stability problems, some additives such as cellulose, epoxy and polymer were mixed into carbon materials, but the existence of the solvents and the insulating additives were found to limit the carrier transport and negatively affect the perovskite/carbon interface [37,38].

In this work, we develop a high performance, stable and low-cost mesoscopic C-PSCs using a thin poly(3-hexylthiophene) (P3HT) layer modified-CNTs (CNTs@P3HT) as the counter electrode. Unlike the commonly used organic HTM, the surface-functionalized CNTs with an extremely low concentration of P3HT (2 mg/mL) can play multiple roles in the C-PSCs: 1) the thin P3HT layer serves as polymer binder to tightly bind the CNTs together through the strong π-π interaction to form a three-dimensional cross-linked structure so as to improve the compactness, conductivity and perovskite interface contact of the carbon electrode film, 2) the thin P3HT modifier acts as an electron blocker to inhibit electron transfer into CNT due to its higher lowest unoccupied molecular orbital (LUMO) energy level than the conduction band edge of the perovskite, and 3) the hydrophobic property of P3HT and CNTs together with the compactness of the film greatly enhance the moisture resistance and thus the overall cell stability. By carefully comparing the performance of the PSCs based on the CNTs@P3HT, the pure CNTs and the conventional sandwiched P3HT/CNTs, we find that the synergistic effect of the P3HT and CNTs greatly improves the performance of the CNTs@P3HT based C-PSCs. By tuning the concentration of the P3HT modifier, the PCEs of the CNTs@P3HT based PSCs have been raised to 13.43% with an average efficiency of 12.54%, which is much higher than the pure CNTs based C-PSCs (best PCE 10.59%) and the sandwich-type P3HT/CNTs based C-PSCs (best PCE 9.50%). What is more, with the CNTs@P3HT electrodes, the cell hysteresis has been significantly reduced and the cell stability has been considerably increased.

2 Experimental

2.1 Materials

Titanium diisopropoxide bis(acetylacetonate) (Tiaca, 75 wt % in isopropanol), ethanol (absolute), lead (II) nitrate ($Pb(NO_3)_2$), potassium iodide (KI), methylamine (MA, 40% in methanol), hydroiodic acid (HI, 57 wt% in water), *N,N*-dimethylformamide (DMF, 99%), Dimethyl sulfoxide (DMSO, 99.9%), cyclohexane (99.7%), *2*-isopropanol (IPA, 99.9%), chlorobenzene (99.8%), P3HT (445703 Aldrich regioregularity⩾90%) and multi-wall carbon nanotube (773840 Aldrich, ⩾98% carbon basis) were purchased from Sigma-Aldrich and directly used without treatment or purification. TiO_2 paste was purchased from Dyesol Australia Pty Ltd.

2.2 C-PSCs fabrication

The PbI_2 and CH_3NH_3I were synthesized using a previously described method [33]. Transparent conducting substrate FTO was first cleaned in ultrasonic bath by detergent solution, water, ethanol, and acetone for 15 min, respectively. Then the washed FTO was dried with clean dry air. For the TiO_2 compact layer (c-TiO_2), a 50 nm thick TiO_2 compact layer was deposited on FTO by a home-made ultrasonic spray deposition system at 500°C using 0.05 M[1)] of Tiaca solution in ethanol (1 mL of Tiaca solution and 39 mL of ethanol) as precursor and dry N_2 as carrier gas [39]. For the mesoporous TiO_2 layer (m-TiO_2), the TiO_2 paste was diluted with 2.5 times of ethanol by weight and was stirred 30 min. Then the diluted TiO_2 paste was spin-coated on the compact TiO_2 layer at 5000 r/min for 30 s. After spinning, the film was dried at 120°C for 5 min and calcination at 500°C for 2 h. $CH_3NH_3PbI_3$ was formed using a modified two-step procedure. First, 1.4 M of PbI_2 solution was prepared by dissolving 461 mg PbI_2 in 0.07 mL of DMSO and 0.63 mL of DMF at 70°C. The FTO/c-TiO_2/m-TiO_2 substrate was heated at 70°C for 10 min before the deposition of PbI_2. 40 μL of PbI_2 solution was spin-coated on the TiO_2 film at 2000 r/min for 20 s (with loading time of 20 s). After spinning, the film was dried at room temperature (R_m). The CH_3NH_3I solution was prepared by adding 40 mg of CH_3NH_3I

1) 1 M = 1 mol/L

(1 mg/mL) in 40 mL of 2-isopropanol/cyclohexene (1/9 v/v) mixture solution. Then the PbI_2-coated substrate was immersed in the CH_3NH_3I solution for 12 h at R_m. Then the dark-brown substrate was picked out and dried at 100°C for 10 min in dry air atmosphere (humidity ~ 10% – 20%). After cooling to R_m, the devices were completed by depositing CNTs@P3HT solutions on the perovskite films by the drop-casting method, followed by heating at 50°C for 10 min and 100°C for 20 min in N_2. For the CNTs@P3HT solutions, different concentrations (1, 2 and 5 mg/mL) of P3HT and 10 mg/mL CNTs were dispersed in chlorobenzene by sonification for 20 min and stir for 5 min. For the sandwiched P3HT/CNTs based C-PSCs, 2 mg/mL of P3HT in chlorobenzene was spin-coated on the perovskite film at 2000 r/min for 20 s, and then 10 mg/mL CNTs in chlorobenzene was drop-casting on the film, followed by heating at 50°C for 10 min and 100°C for 20 min in N_2. Devices were measured under simulated AM 1.5 G, 100 mW/cm^2 sunlight with an active area of 0.08 cm^2.

2.3 Characterization

X-Ray diffraction (XRD) data was collected on an X'pert Pro (PANalytical) with Cu Ka radiation. Morphologies of films were examined by JEOL6700F scanning electron microscope (SEM) at an accelerating voltage of 5 kV. Raman spectra were recorded on LabRAM HR Raman microscope with a laser excitation wavelength of 514.5 nm. Current density-voltage (*J-V*) characteristic curves were recorded using an IM6x electrochemical workstation (ZAHNER-Elektrik GmbH & Co., KG, Germany). Incident-photon-to current conversion efficiency (IPCE) spectra were recorded using IPCE kit developed by ZAHNER-Elektrik in AC mode with frequency of 1 Hz.

3 Results and discussion

The fabrication procedures of the mesoscopic C-PSCs are shown in Fig. 1. The $CH_3NH_3PbI_3$ perovskite film is deposited by a modified two-step sequential method (Experimental section, Section 2), and the SEM images and XRD pattern of the $CH_3NH_3PbI_3$ films are shown in Fig. 2. The high quality, uniform and closely packed perovskite crystalline films are prerequisite for high photovoltaic performance [40]. Here three types of structures based on different CNTs cathodes are studied. The CNTs@P3HT based C-PSCs is shown in Fig. 1(a), and for comparison, the pure CNTs and sandwiched P3HT/CNTs based C-PSCs are shown in Figs. 1(b) and 1(c), respectively. To form the structure of CNTs@P3HT based C-PSCs, a low concentration of P3HT is dissolved in the CNTs chlorobenzene suspension, which is then drop-cast onto the pre-formed perovskite surface resulting in a thin P3HT layer modified CNTs electrode (see the close-ups on the right side of Fig. 1), while in the sandwiched P3HT/CNTs based C-PSCs, the P3HT film and CNTs film are deposited on the perovskite layer successively.

The comparison of the SEM images of three different types of CNTs cathodes based C-PSCs is shown in Fig. 3. It should be note that the thin P3HT layer cannot be easily distinguished from the SEM images. As regards the CNTs@P3HT cathode based C-PSCs shown in Fig. 3(a), a seamless and continuous CNTs film is formed on the perovskite surface. The corresponding cross-sectional SEM image in Fig. 3(b) show that the CNTs tend to pack compactly and connect with each other forming a continuous layered film, and the CNTs film strongly attach on the perovskite surface. The total thickness of the compact CNTs@P3HT cathode is ~40 μm. Nevertheless, for the pure CNTs and sandwiched P3HT/CNTs based

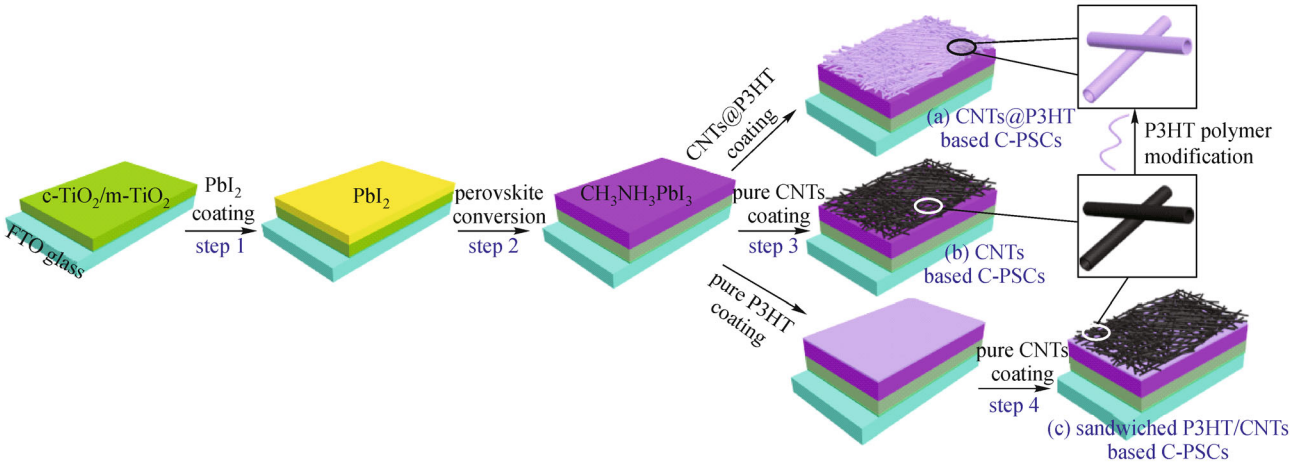

Fig. 1 Schematic showing the fabrication processes of (a) CNTs@P3HT based C-PSCs, (b) CNTs based C-PSCs, and (c) sandwiched P3HT/CNTs based C-PSCs

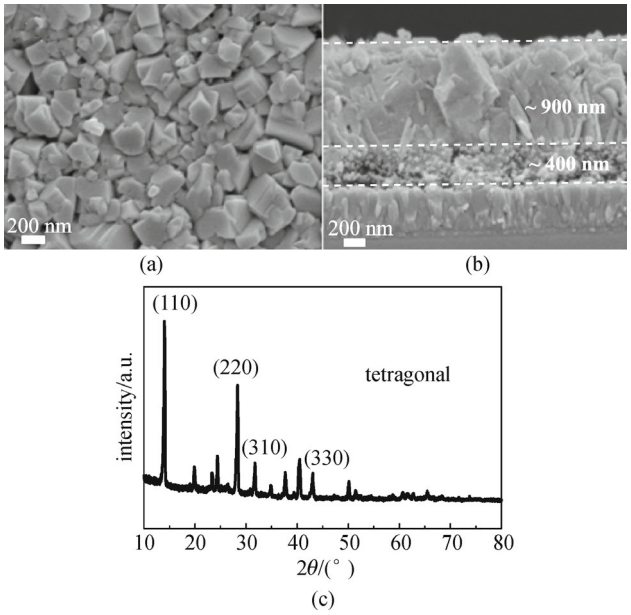

Fig. 2 (a) Top view and (b) cross sectional view SEM images of $CH_3NH_3PbI_3$ film on FTO glass/c-TiO_2/m-TiO_2, showing that the size of the crystals is in the range of ~250–400 nm, the thickness of the m-TiO_2/perovskite is ~400 nm, and the thickness of the perovskite capping layer is ~900 nm. (c) XRD pattern of the $CH_3NH_3PbI_3$ film on FTO glass/c-TiO_2/m-TiO_2

structures, relatively rough CNTs films are formed on the perovskite surface (the SEM images shown in Figs. 3(c)–3(f)), and the CNTs are loosely packed and obvious gaps and large aggregates can be seen. It indicates that the presence of thin P3HT layer can significantly improve the film-formation ability of CNTs and the P3HT can serve as polymer binder to tightly bind the CNTs together to form a three-dimensional cross-linked structure, which can work as charge transport highway for holes and should be beneficial to the solar cell performance. While for the pure CNTs film, there is no binder between the CNTs and the van der Waals force is not strong enough to make the CNTs pack closely. The CNTs tend to aggregate severely after the evaporation of solvent, leaving behind many gaps between the perovskite and CNTs films. In this case, the hole extraction from the perovskite to the CNTs electrode can be encumbered and the transport of the holes through the CNTs film is expected to be slow.

To investigate the interaction between the P3HT and CNTs of the CNTs@P3HT, Raman spectra and XRD patterns of pure P3HT, pure CNTs, and CNTs@P3HT films were collected (Figs. 4(a) and 4(b)). As shown in Fig. 4(a), to the pure P3HT, the predominant two peaks at 1379 and 1450 cm^{-1} are assigned to the C-C and C = C stretching vibration, respectively [41,42]. The pure CNTs yield a Raman spectrum containing a G band (1578 cm^{-1}) of sp^2 carbon, along with a D band (1342 cm^{-1}) of sp^3 carbon and a G′ band (2683 cm^{-1}) of graphite [43]. In the case of the CNTs@P3HT film, the D band peak and G band peak of CNTs are shifted to higher frequency (1345 cm^{-1}) and lower frequency (1575 cm^{-1}), respectively, compared with the pure CNTs. Meanwhile, the G′ band peak is shifted to low frequency (2679 cm^{-1}). According to previous studies, the shift of the G band and G′ band can be derived from the strong π-π interaction and charge transfer between P3HT and CNTs [44–46]. Moreover, the Raman peak of P3HT in the CNTs@P3HT film is also shifted from 1450 to 1443 cm^{-1}, further indicating the strong interaction between the thin P3HT layer and CNTs [47]. Figure 4(b) shows the XRD patterns for the pure P3HT film, pure CNTs and CNTs@P3HT films. The peak at 25.6° in the CNTs and

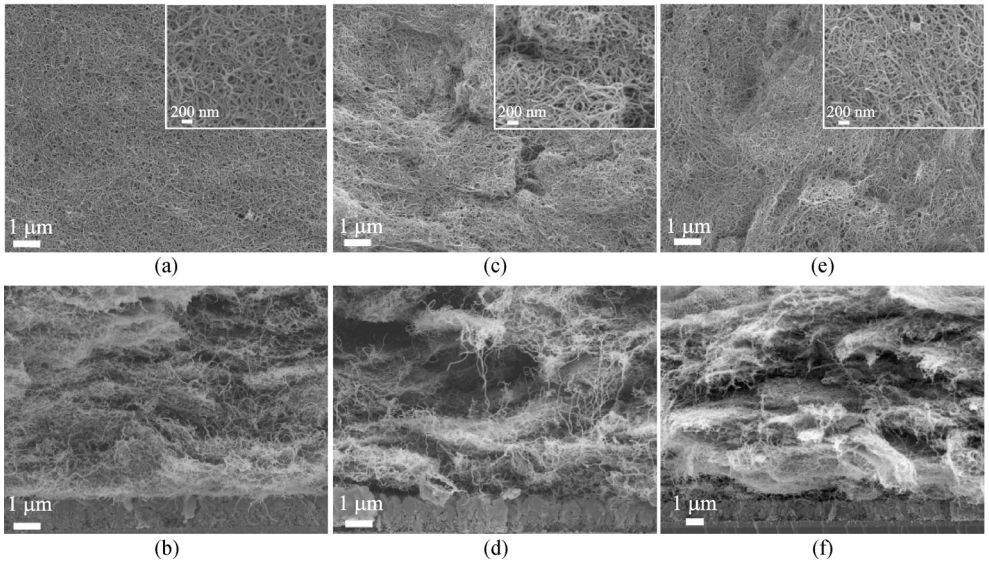

Fig. 3 SEM images of (a, b) CNTs@P3HT based C-PSCs, (c, d) CNTs based C-PSCs, and (e, f) sandwiched P3HT/CNTs based C-PSCs. The concentration of P3HT is 2 mg/mL and the concentration of CNTs is 10 mg/mL in chlorobenzene

CNTs@P3HT samples is attributed to the characteristic peak of the CNTs [48]. In the case of the pristine P3HT thin film, the strong Bragg peak at 5.2° is assigned to (100) of P3HT derived from lamellar layer structure. However, as the CNTs@P3HT film, the intensity of the (100) peak is significantly reduced (inset in Fig. 4(b)), indicating the presence of the CNTs influence the molecular ordering of the P3HT [49]. It is thus conceivable that the thin P3HT layer cannot only act as polymer binder to tightly bound the CNTs together to improve the compactness of the carbon electrode film as well as the interface with perovskite layer, but also the relatively strong π-π interaction between the P3HT and CNTs endow rapid carrier transport. Besides, the thin P3HT modifier can also act as an electron blocker inhibiting electron transfer into CNT due to favorable energy level alignment. Figure 4(c) present the energy-level diagram of CNTs@P3HT based C-PSC [25,33,50,51]. Thanks to the ambipolar property of $CH_3NH_3PbI_3$ perovskite, electrons can inject effectively into the conductive band of m-TiO_2, and the holes can be collected by the CNTs@P3HT electrode [12,16]. Due to the hole-transporting property of P3HT and the suitable energy-level alignment, the thin P3HT layer can efficiently extract the holes, facilitate the carrier separation and restrain photogenerated carrier recombination [52]. Moreover, the holes can be efficiently transported from P3HT to CNTs due to the strong π-π interaction and the three-dimensional cross-linked network of CNTs.

To evaluate the photovoltaic performance of the different CNTs cathodes based C-PSCs, the photocurrent-voltage (*J-V*) curves of the PSCs under AM 1.5 illumination of 100 mW/cm^2 are recorded and presented in Fig. 5(a). It is well established that the interfacial contact between perovskite and CNTs cathode and the conductivity of the cathode are vital for charge separation and transfer in PSCs. The PSCs based on the sandwiched P3HT/CNTs cathode exhibits the lowest performance with an V_{oc} of 0.85 V, J_{sc} of 18.62 mA/cm^2, *FF* of 0.60, and PCE of 9.50%, which is mainly attributed to extremely low hole mobility (~1 × 10^{-4} cm^2/(V·S)) without doping [52–54]. When using the pure CNTs as the cathode, the performance is increased (V_{oc} of 0.82 V, J_{sc} of 20.49 mA/cm^2, *FF* of 0.63, and PCE of 10.59%), demonstrating that the CNTs can replace both HTM and metal due to their outstanding conductivity and suitable energy level. However, due to the loosely packed CNTs film together with the poor interface with perovskite, the V_{oc} is relatively low. When the thin P3HT layer is introduced onto the CNTs surface, the cell performances are dramatically enhanced. For the CNTs@P3HT based cells, the V_{oc} is improved to 0.91 V, the J_{sc} is increased to 22.71 mA/cm^2 and the *FF* is improved to 0.65, yielding 13.43% of PCE. This points to

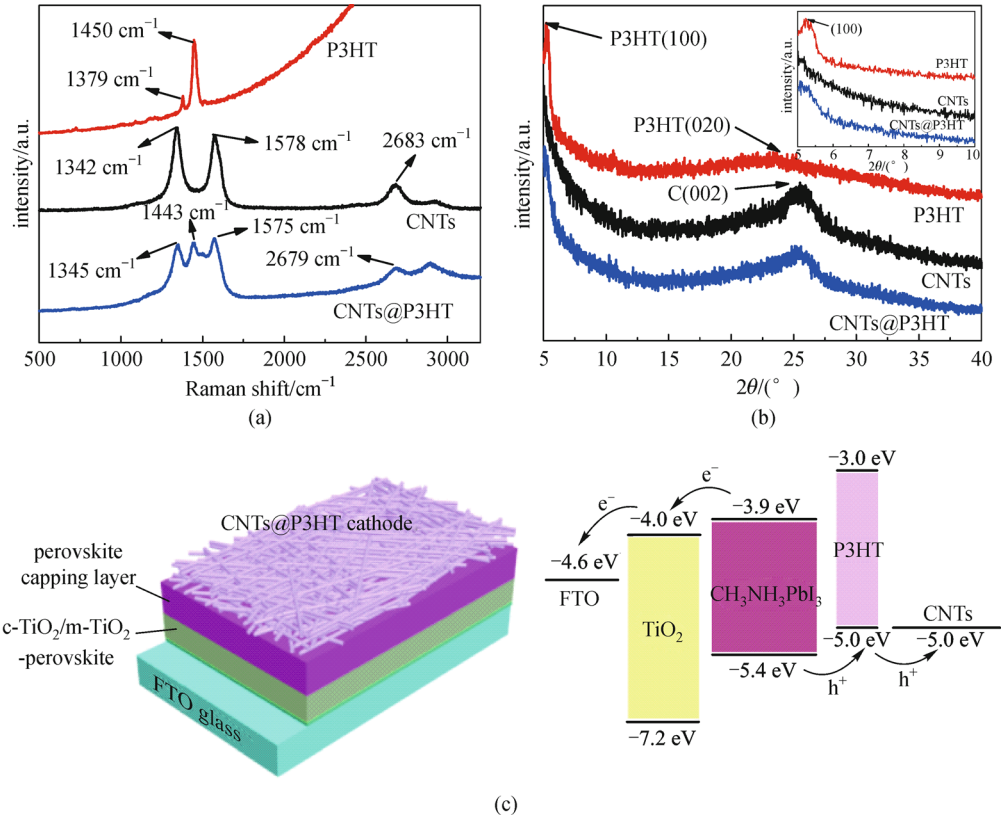

Fig. 4 (a) Raman spectra and (b) XRD patterns of pure P3HT, pure CNTs, and CNTs@P3HT films (2 mg/mL of P3HT). The inset in (b) shows magnified XRD patterns in the 5°–10° region. (c) Device configuration (left) and energy band diagram (right) of CNTs@P3HT based C-PSCs

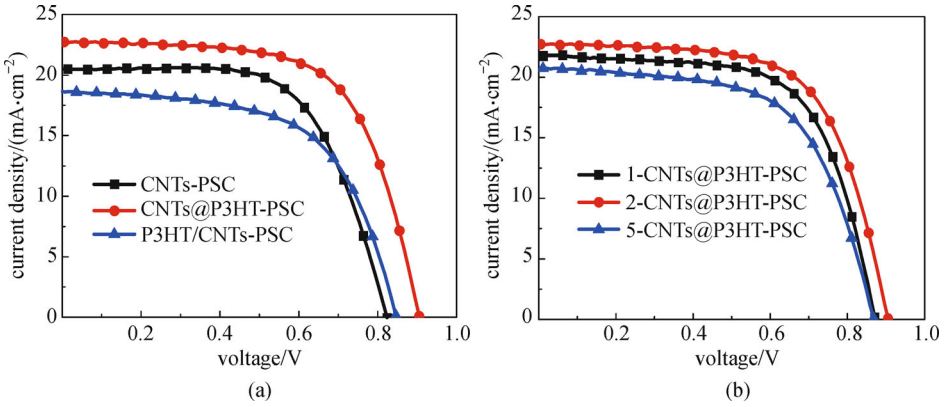

Fig. 5 (a) *J-V* curves of the C-PSCs with pure CNTs, CNTs@P3HT and sandwiched P3HT/CNTs cathodes (2 mg/mL of P3HT and 10 mg/mL CNTs); (b) *J-V* curves of the CNTs@P3HT based C-PSCs with different concentrations of P3HT (1, 2 and 5 mg/mL)

the synergistic effects of the P3HT and the CNTs wherein the thin P3HT layer serves as polymer binder and electron blocker and the CNTs network provides the conductive pathways. Moreover, the concentration of the P3HT also has a significant influence on the PSCs performance. For this experiment, we use the same amount of CNTs but three different concentrations of P3HT are added, which are 1, 2 and 5 mg/mL, respectively. *J-V* curves of the CNTs@P3HT based PSCs with different concentrations of P3HT are presented in Fig. 5(b). Obviously, the performances of all the CNTs@P3HT based PSCs are improved compared with the pure CNTs-PSCs, especially for the V_{oc} and J_{sc} mainly due to the increased compactness of the CNTs film and good interface with perovskite thanks to the thin P3HT layer. However, the V_{oc} and J_{sc} of the 1-CNTs@P3HT-PSCs (V_{oc} of 0.87 V, J_{sc} of 21.75 mA/cm^2, *FF* of 0.65, and PCE of 12.30%) are lower than that of the 2-CNTs@P3HT-PSCs, suggesting that extremely low concentration of P3HT is not enough to connect the CNTs together to form three-dimensional cross-linked CNTs network. When further increasing the P3HT content (5 mg/mL), lower cell performance is obtained (V_{oc} of 0.87 V, J_{sc} of 20.72 mA/cm^2, *FF* of 0.61, and PCE of 11.00%), which mainly owing to too much P3HT will block the conductive pathway and thus strong recombination. Therefore, 2 mg/mL of P3HT has been regarded as the optimal concentration in the CNTs@P3HT cathode based PSCs. To check the reproducibility of the PSCs, the data of a batch of 20 devices for each sample are collected and summarized in Table 1.

To examine the possible hysteresis in the devices, the *J-V* curves of the champion PSC based on the CNTs@P3HT cathode (2 mg/mL P3HT) are further measured via the forward and backward scans with a san rate of 10 mV/s (Fig. 6(a)). Obviously, the CNTs@P3HT cathode based PSCs show negligible hysteresis, with the forward scan PCE of 13.01% and reverse scan PCE of 13.43%, further proving the favorable charge transport and intimate interface with perovskite provided by the novel CNTs@P3HT cathode. Figure 6(b) shows the IPCE spectrum for the CNTs@P3HT-PSC. Integrating the overlap of the IPCE spectrum yield a photocurrent density of 20.76 mA/cm^2, which is in agreement with the measured photocurrent density (Fig. 5(a)). Beyond the efficiency, the stability is also the key for the commercialization of the PSCs. We record the photocurrent density of the CNTs@P3HT-PSC at a function of time held at a maximum output power point (Fig. 6(c)), which is a useful parameter to present the cell performance and stability [55]. As shown in Fig. 6(c), the device exhibit a fast photo-response to light on and off and the photocurrent density stabilizes quickly at around 19.10 mA/cm^2, indicating fast charge transfer in the C-PSC. Moreover, the stability of the CNTs@P3HT-PSC at ambient condition is also recorded and the stability of the CNTs-PSC is also present for comparison (Fig. 6(d)). It should be note that some increase in the PCEs occur at the first few days, which might be resulted from the improved interface and

Table 1 Photovoltaic performance summarization of C-PSCs based on different cathodes and different concentrations of P3HT. The data and statistics are based on 20 devices for each type

samples	V_{oc}/V	J_{sc}/(mA·cm^{-2})	*FF*	PCE/%	best PCE/%
CNTs-PSCs	0.82±0.01	20.14±1.85	0.60±0.04	9.91±0.53	10.59
P3HT/CNTs-PSCs	0.83±0.02	18.66±1.26	0.55±0.02	8.47±0.64	9.50
1-CNTs@P3HT-PSCs	0.86±0.02	21.12±0.83	0.62±0.03	11.25±0.63	12.30
2-CNTs@P3HT-PSCs	0.90±0.02	22.21±0.77	0.63±0.02	12.54±0.51	13.43
5-CNTs@P3HT-PSCs	0.86±0.02	20.25±1.06	0.59±0.03	10.27±0.52	11.00

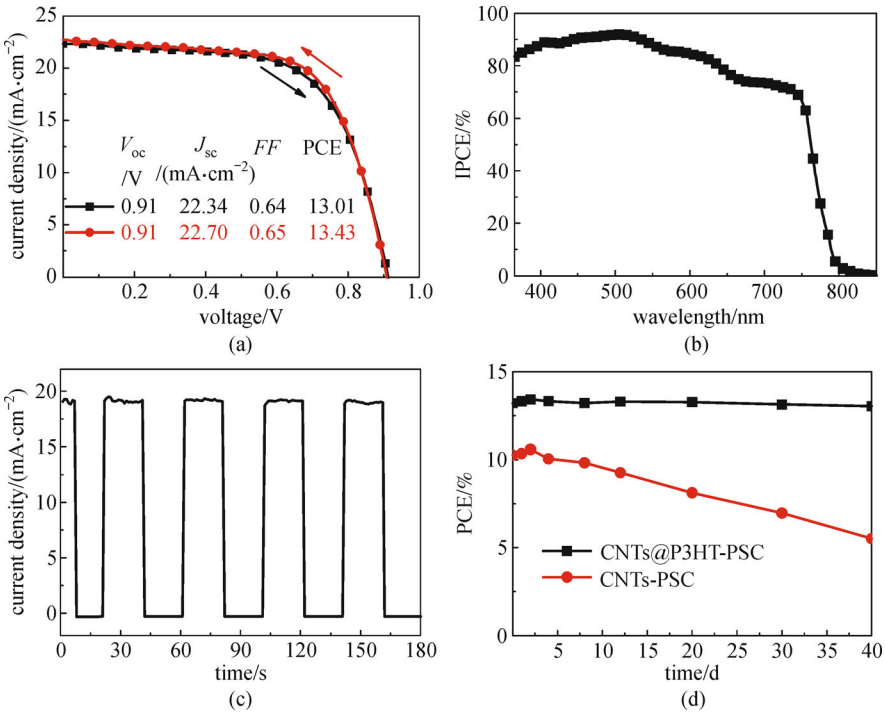

Fig. 6 (a) *J-V* curves for the champion CNTs@P3HT-PSC measured with different scanning directions: forward scan from 0 V to V_{oc} (black curve) and reverse scan from V_{oc} to 0 V (red curve); (b) the corresponding IPCE spectrum of the CNTs@P3HT-PSC; (c) photocurrent density as a function of time held at the maximum output power point (0.70 V) under on-off illumination cycles for the CNTs@P3HT-PSC; (d) the efficiencies of the champion CNTs@P3HT-PSC and the champion CNTs-PSC as a function of storage time in the ambient atmosphere (temperature 25°C, humidity ~20%–40%). The concentration of P3HT is 2 mg/mL

stress release during the storage [19]. In the whole testing process, a slight PCE decrease is observed and the PCE of the CNTs@P3HT-PSC change from 13.43% to 13.04% with a 3% drop during 40 days' storage. However, the CNTs-PSC exhibit inferior stability and the PCE drops from 10.59% to 5.52% with a 48% drop at the same storage condition. Thus, the remarkable stability of the CNTs@P3HT-PSC is attributed to the thin P3HT layer on the CNTs surface, which serves as polymer binder to tightly bind the CNTs together to improve the compactness of the carbon electrode film (Figs. 3(a) and 3(b)) as well as the hydrophobic property of P3HT and CNTs greatly ameliorate the stability of the solar cell [56,57]. Therefore, we believe that the CNTs@P3HT-PSCs provide a stable and low cost strategy for high efficiency PSCs.

4 Conclusions

In conclusion, a high performance, low cost and stable CNTs@P3HT cathode based mesoscopic C-PSC has been fabricated by a simple process. By comparison with the pure CNTs based C-PSCs and conventional sandwiched P3HT/CNTs based C-PSCs, it is revealed that the thin P3HT modifier on CNTs has significant beneficial influence on the CNTs cathode and the overall cell performance of the CNTs@P3HT based C-PSCs. The CNTs film is found to be packed densely in the presence of the P3HT modifier, forming three-dimensional cross-linked conductive pathways and intimate interfaces with the perovskite layer. Fast hole transport and reduced recombination have been achieved due to the strong π-π interaction between the P3HT layer and CNTs as well as the high LUMO energy level of P3HT for blocking the conduction band electrons. What's more, the compact CNTs@P3HT cathode together with the hydrophobic property of P3HT and CNTs greatly improve the stability of the solar cell. Through careful optimizations of the surface modified CNTs cathodes by varying the concentrations of the P3HT modifier, we found that the PSCs based on the CNTs@P3HT cathode with 2 mg/mL of P3HT present the best cell performance with a PCE of up to 13.43% and an average efficiency of 12.54%.

Acknowledgements This work was supported by the HK Innovation and Technology Fund (ITS/004/14) and the HK-RGC General Research Funds (GRE No. HKUST 606511).

References

1. Kojima A, Teshima K, Shirai Y, Miyasaka T. Organometal halide perovskites as visible-light sensitizers for photovoltaic cells. Journal

of the American Chemical Society, 2009, 131(17): 6050–6051
2. Kim H S, Lee C R, Im J H, Lee K B, Moehl T, Marchioro A, Moon S J, Humphry-Baker R, Yum J H, Moser J E, Grätzel M, Park N G. Lead iodide perovskite sensitized all-solid-state submicron thin film mesoscopic solar cell with efficiency exceeding 9%. Scientific Reports, 2012, 2: 591
3. Liu M, Johnston M B, Snaith H J. Efficient planar heterojunction perovskite solar cells by vapour deposition. Nature, 2013, 501 (7467): 395–398
4. Burschka J, Pellet N, Moon S J, Humphry-Baker R, Gao P, Nazeeruddin M K, Grätzel M. Sequential deposition as a route to high-performance perovskite-sensitized solar cells. Nature, 2013, 499(7458): 316–319
5. Park N G. Organometal perovskite light absorbers toward a 20% efficiency low-cost solid-state mesoscopic solar Cell. Journal of Physical Chemistry Letters, 2013, 4(15): 2423–2429
6. Zhou H, Chen Q, Li G, Luo S, Song T B, Duan H S, Hong Z, You J, Liu Y, Yang Y. Interface engineering of highly efficient perovskite solar cells. Science, 2014, 345(6196): 542–546
7. Jeon N J, Noh J H, Kim Y C, Yang W S, Ryu S, Seok S I. Solvent engineering for high-performance inorganic-organic hybrid perovskite solar cells. Nature Materials, 2014, 13(9): 897–903
8. Li X, Dar M I, Yi C, Luo J, Tschumi M, Zakeeruddin S M, Nazeeruddin M K, Han H, Grätzel M. Improved performance and stability of perovskite solar cells by crystal crosslinking with alkylphosphonic acid ω-ammonium chlorides. Nature Chemistry, 2015, 7(9): 703–711
9. Tress W, Marinova N, Moehl T, Zakeeruddin S M, Nazeeruddin M K, Gratzel M. Understanding the rate-dependent *J-V* hysteresis, slow time component, and aging in $CH_3NH_3PbI_3$ perovskite solar cells: the role of a compensated electric field. Energy & Environmental Science, 2015, 8(3): 995–1004
10. Roldán-Carmona C, Gratia P, Zimmermann I, Grancini G, Gao P, Graetzel M, Nazeeruddin M K. High efficiency methylammonium lead triiodide perovskite solar cells: the relevance of non-stoichiometric precursors. Energy & Environmental Science, 2015, 8(12): 3550–3556
11. Yang W S, Noh J H, Jeon N J, Kim Y C, Ryu S, Seo J, Seok S I I. High-performance photovoltaic perovskite layers fabricated through intramolecular exchange. Science, 2015, 348(6240): 1234–1237
12. Etgar L, Gao P, Xue Z, Peng Q, Chandiran A K, Liu B, Nazeeruddin M K, Grätzel M. Mesoscopic $CH_3NH_3PbI_3/TiO_2$ heterojunction solar cells. Journal of the American Chemical Society, 2012, 134 (42): 17396–17399
13. Laban W A, Etgar L. Depleted hole conductor-free lead halide iodide heterojunction solar cells. Energy & Environmental Science, 2013, 6(11): 3249–3253
14. Batmunkh M, Shearer C J, Biggs M J, Shapter J G. Nanocarbons for mesoscopic perovskite solar cells. Journal of Materials Chemistry A, Materials for Energy and Sustainability, 2015, 3(17): 9020–9031
15. Habisreutinger S N, Leijtens T, Eperon G E, Stranks S D, Nicholas R J, Snaith H J. Carbon nanotube/polymer composites as a highly stable hole collection layer in perovskite solar cells. Nano Letters, 2014, 14(10): 5561–5568
16. Ku Z, Rong Y, Xu M, Liu T, Han H. Full printable processed mesoscopic $CH_3NH_3PbI_3/TiO_2$ heterojunction solar cells with carbon counter electrode. Scientific Reports, 2013, 3: 3132
17. Wang J T W, Ball J M, Barea E M, Abate A, Alexander-Webber J A, Huang J, Saliba M, Mora-Sero I, Bisquert J, Snaith H J, Nicholas R J. Low-temperature processed electron collection layers of graphene/TiO_2 nanocomposites in thin film perovskite solar cells. Nano Letters, 2014, 14(2): 724–730
18. Cao J, Liu Y M, Jing X, Yin J, Li J, Xu B, Tan Y Z, Zheng N. Well-defined thiolated nanographene as hole-transporting material for efficient and stable perovskite solar cells. Journal of the American Chemical Society, 2015, 137(34): 10914–10917
19. Wei H Y, Xiao J Y, Yang Y Y, Lv S T, Shi J J, Xu X, Dong J, Luo Y H, Li D M, Meng Q B. Free-standing flexible carbon electrode for highly efficient hole-conductor-free perovskite solar cells. Carbon, 2015, 93: 861–868
20. Liu L, Mei A, Liu T, Jiang P, Sheng Y, Zhang L, Han H. Fully printable mesoscopic perovskite solar cells with organic silane self-assembled monolayer. Journal of the American Chemical Society, 2015, 137(5): 1790–1793
21. Wei Z, Chen H, Yan K, Yang S. Inkjet printing and instant chemical transformation of a $CH_3NH_3PbI_3$/nanocarbon electrode and interface for planar perovskite solar cells. Angewandte Chemie (International Edition), 2014, 53(48): 13239–13243
22. Yan K, Wei Z, Li J, Chen H, Yi Y, Zheng X, Long X, Wang Z, Wang J, Xu J, Yang S. High-performance graphene-based hole conductor-free perovskite solar cells: Schottky junction enhanced hole extraction and electron blocking. Small, 2015, 11(19): 2269–2274
23. Zhou H W, Shi Y T, Wang K, Dong Q S, Bai X G, Xing Y J, Du Y, Ma T L. Low-temperature processed and carbon-based ZnO/$CH_3NH_3PbI_3$/C planar heterojunction perovskite solar cells. Journal of Physical Chemistry C, 2015, 119(9): 4600–4605
24. Wu Z, Bai S, Xiang J, Yuan Z, Yang Y, Cui W, Gao X, Liu Z, Jin Y, Sun B. Efficient planar heterojunction perovskite solar cells employing graphene oxide as hole conductor. Nanoscale, 2014, 6 (18): 10505–10510
25. Li Z, Kulkarni S A, Boix P P, Shi E, Cao A, Fu K, Batabyal S K, Zhang J, Xiong Q, Wong L H, Mathews N, Mhaisalkar S G. Laminated carbon nanotube networks for metal electrode-free efficient perovskite solar cells. ACS Nano, 2014, 8(7): 6797–6804
26. Xu X, Liu Z, Zuo Z, Zhang M, Zhao Z, Shen Y, Zhou H, Chen Q, Yang Y, Wang M. Hole selective NiO contact for efficient perovskite solar cells with carbon electrode. Nano Letters, 2015, 15(4): 2402–2408
27. Wei Z H, Chen H N, Yan K Y, Zheng X L, Yang S H. Hysteresis-free multi-wall carbon nanotube-based perovskite solar cells with a high fill factor. Journal of Materials Chemistry A, 2015, doi: 10.1039/C5TA07714A
28. Rong Y G, Liu L F, Mei A Y, Li X, Han H W. Beyond efficiency: the challenge of stability in mesoscopic perovskite solar cells. Advanced Energy Materials, 2015, 5(20): 1501066
29. Mei A, Li X, Liu L, Ku Z, Liu T, Rong Y, Xu M, Hu M, Chen J, Yang Y, Grätzel M, Han H. A hole-conductor-free, fully printable mesoscopic perovskite solar cell with high stability. Science, 2014, 345(6194): 295–298

30. Xu M, Rong Y, Ku Z, Mei A, Liu T, Zhang L, Li X, Han H. Highly ordered mesoporous carbon for mesoscopic $CH_3NH_3PbI_3/TiO_2$ heterojunction solar cell. Journal of Materials Chemistry A, Materials for Energy and Sustainability, 2014, 2(23): 8607–8611
31. Zhang L, Liu T, Liu L, Hu M, Yang Y, Mei A, Han H. The effect of carbon counter electrodes on fully printable mesoscopic perovskite solar cells. Journal of Materials Chemistry. A, Materials for Energy and Sustainability, 2015, 3(17): 9165–9170
32. Liu T, Liu L, Hu M, Yang Y, Zhang L, Mei A, Han H. Critical parameters in TiO_2/ZrO_2/carbon-based mesoscopic perovskite solar cell. Journal of Power Sources, 2015, 293: 533–538
33. Wei Z H, Yan K Y, Chen H N, Yi Y, Zhang T, Long X, Li J K, Zhang L X, Wang J N, Yang S H. Cost-efficient clamping solar cells using candle soot for hole extraction from ambipolar perovskites. Energy & Environmental Science, 2014, 7(10): 3326–3333
34. Yang Y, Xiao J, Wei H, Zhu L, Li D, Luo Y, Wu H, Meng Q. An all-carbon counter electrode for highly efficient hole-conductor-free organo-metal perovskite solar cells. RSC Advances, 2014, 4(95): 52825–52830
35. Zhou H, Shi Y, Dong Q, Zhang H, Xing Y, Wang K, Du Y, Ma T. Hole-conductor-free, metal-electrode-free $TiO_2/CH_3NH_3PbI_3$ heterojunction solar cells based on a low-temperature carbon electrode. Journal of Physical Chemistry Letters, 2014, 5(18): 3241–3246
36. Zhang F, Yang X, Wang H, Cheng M, Zhao J, Sun L. Structure engineering of hole-conductor free perovskite-based solar cells with low-temperature-processed commercial carbon paste as cathode. ACS Applied Materials & Interfaces, 2014, 6(18): 16140–16146
37. Chen H N, Wei Z H, Zheng X L, Yang S H. A scalable electrodeposition route to the low-cost, versatile and controllable fabrication of perovskite solar cells. Nano Energy, 2015, 15: 216–226
38. Zheng X L, Wei Z H, Chen H N, Bai Y, Xiao S, Zhang T, Yang S H. In-situ fabrication of dual porous titanium dioxide films as anode for carbon cathode based perovskite solar cell. Journal of Energy Chemistry, 2015, doi: 10.1016/j.jechem.2015.10.003
39. Wei Z H, Zheng X L, Chen H N, Long X, Wang Z L, Yang S H. A multifunctional C plus epoxy/Ag-paint cathode enables efficient and stable operation of perovskite solar cells in watery environments. Journal of Materials Chemistry A, Materials for Energy and Sustainability, 2015, 3(32): 16430–16434
40. Hao F, Stoumpos C C, Liu Z, Chang R P H, Kanatzidis M G. Controllable perovskite crystallization at a gas-solid interface for hole conductor-free solar cells with steady power conversion efficiency over 10%. Journal of the American Chemical Society, 2014, 136(46): 16411–16419
41. Meng D L, Sun J H, Jiang S D, Zeng Y, Li Y, Yan S K, Geng J X, Huang Y. Grafting P3HT brushes on GO sheets: distinctive properties of the GO/P3HT composites due to different grafting approaches. Journal of Materials Chemistry, 2012, 22(40): 21583–21591
42. Xiao J Y, Shi J J, Liu H B, Xu Y Z, Lv S T, Luo Y H, Li D M, Meng Q B, Li Y L. Efficient $CH_3NH_3PbI_3$ perovskite solar cells based on graphdiyne (GD)-modified P3HT hole-transporting material. Advanced Energy Materials, 2015, 5(8): 1401943
43. Eklund P C, Holden J M, Jishi R A. Vibrational-modes of carbon nanotubes- spectroscopy and theory. Carbon, 1995, 33(7): 959–972
44. Yang D Q, Rochette J F, Sacher E. Spectroscopic evidence for π-π interaction between poly(diallyl dimethylammonium) chloride and multiwalled carbon nanotubes. Journal of Physical Chemistry B, 2005, 109(10): 4481–4484
45. Rao A M, Eklund P C, Bandow S, Thess A, Smalley R E. Evidence for charge transfer in doped carbon nanotube bundles from Raman scattering. Nature, 1997, 388(6639): 257–259
46. D'Urso L, Forte G, Russo P, Caccamo C, Compagnini G, Puglisi O. Surface-enhanced raman scattering study on 1D–2D graphene-based structures. Carbon, 2011, 49(10): 3149–3157
47. Chen J, Liu H, Weimer W A, Halls M D, Waldeck D H, Walker G C. Noncovalent engineering of carbon nanotube surfaces by rigid, functional conjugated polymers. Journal of the American Chemical Society, 2002, 124(31): 9034–9035
48. Jiang L Q, Gao L. Carbon nanotubes-metal nitride composites: a new class of nanocomposites with enhanced electrical properties. Journal of Materials Chemistry, 2005, 15(2): 260–266
49. Park Y D, Lim J A, Jang Y, Hwang M, Lee H S, Lee D H, Lee H J, Baek J B, Cho K. Enhancement of the field-effect mobility of poly (3-hexylthiophene)/functionalized carbon nanotube hybrid transistors. Organic Electronics, 2008, 9(3): 317–322
50. Dou L T, You J B, Yang J, Chen C C, He Y J, Murase S, Moriarty T, Emery K, Li G, Yang Y. Tandem polymer solar cells featuring a spectrally matched low-bandgap polymer. Nature Photonics, 2012, 6(3): 180–185
51. Irwin M D, Buchholz B, Hains A W, Chang R P H, Marks T J. p-Type semiconducting nickel oxide as an efficiency-enhancing anode interfacial layer in polymer bulk-heterojunction solar cells. Proceedings of the National Academy of Sciences of the United States of America, 2008, 105(8): 2783–2787
52. Heo J H, Im S H, Noh J H, Mandal T N, Lim C S, Chang J A, Lee Y H, Kim H J, Sarkar A, Nazeeruddin M K, Gratzel M, Seok S I I. Efficient inorganic-organic hybrid heterojunction solar cells containing perovskite compound and polymeric hole conductors. Nature Photonics, 2013, 7(6): 486–491
53. Bi D, Yang L, Boschloo G, Hagfeldt A, Johansson E M J. Effect of different hole transport materials on recombination in $CH_3NH_3PbI_3$ perovskite-sensitized mesoscopic solar cells. Journal of Physical Chemistry Letters, 2013, 4(9): 1532–1536
54. Ebadian S, Gholamkhass B, Shambayati S, Holdcroft S, Servati P. Effects of annealing and degradation on regioregular polythiophene-based bulk heterojunction organic photovoltaic devices. Solar Energy Materials and Solar Cells, 2010, 94(12): 2258–2264
55. Snaith H J, Abate A, Ball J M, Eperon G E, Leijtens T, Noel N K, Stranks S D, Wang J T W, Wojciechowski K, Zhang W. Anomalous hysteresis in perovskite solar cells. Journal of Physical Chemistry Letters, 2014, 5(9): 1511–1515
56. Bilkay T, Schulze K, Egorov-Brening T, Bohn A, Janietz S. Copolythiophenes with hydrophilic and hydrophobic side chains: synthesis, characterization, and performance in organic field effect transistors. Macromolecular Chemistry and Physics, 2012, 213(18): 1970–1978
57. Hummer G, Rasaiah J C, Noworyta J P. Water conduction through

the hydrophobic channel of a carbon nanotube. Nature, 2001, 414 (6860): 188–190

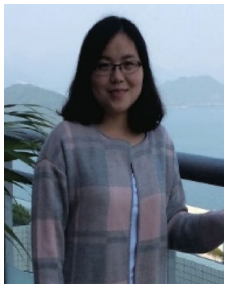

Xiaoli Zheng obtained her M.S. degree in 2012 from Zhengzhou University. She is currently a Ph.D. candidate in Prof. Shihe Yang's group in Department of Chemistry of The Hong Kong University of Science and Technology. Her current research focuses on synthesis of nanomaterials and their applications in perovskite solar cells.

Haining Chen received his Ph.D. degree (2013) in School of Materials Science and Engineering from Beihang University. He is currently a postdoctor in Prof. Shihe Yang's group in Department of Chemistry of The Hong Kong University of Science and Technology. His current research focuses on perovskite solar cells and photoelectrochemical water splitting.

Zhanhua Wei obtained his B.S. degree in 2011 from Xiamen University. He obtained his Ph.D. degree in 2015 in Prof. Shihe Yang's group in Department of Chemistry of The Hong Kong University of Science and Technology. His current research focuses on perovskite solar cells and dye-sensitized solar cells.

Yinglong Yang acquired his B.S. degree in 2013 from University of Science and Technology of China. He is currently a Ph.D. candidate in Prof. Shihe Yang's group in Department of Chemistry of The Hong Kong University of Science and Technology. His current research focuses on carbon based perovskite solar cells.

He Lin received his B.S. degree (2015) in College of Chemistry and Life Science from Zhejiang Normal University. He is currently a research assistant in Prof. Shihe Yang's group in Department of Chemistry of The Hong Kong University of Science and Technology. His current research focuses on hydrogen fuel generation by photoelectrochemical (PEC) water splitting.

Shihe Yang received his B.S. degree in Chemistry from Sun Yat-Sen University and Ph.D. degree in Physical Chemistry (with Prof. Richard E. Smalley). He did his post-doctoral research at Argonne National Laboratory and the University of Toronto (with Prof. John C. Polanyi) before joining the faculty at The Hong Kong University of Science and Technology, where he is currently a full Professor. His current research interests include the understanding, manipulation and applications of low- dimensional nanosystems and energy materials, particularly in novel solar cells and solar fuel devices.